Asian Journal of Chemistry; Vol. 38, No. 3 (2026), 674-682
ASIAN JOURNAL OF CHEMISTRY
https://doi.org/10.14233/ajchem.2026.35254

Green Synthesis, Characterisation and Antibacterial and Anticancer Activities of Palladium-Iridium Bimetallic Nanoparticles using *Murraya koenigii* Leaf Extract

ANJALI GOEL[1], DEEPA SAINI[1,*], SHIKHA[1], MONIKA RANI[2] and POOJA[3]

[1]Department of Chemistry, Kanya Gurukul Haridwar, Gurukul Kangri (Deemed to be University), Haridwar-249407, India
[2]Department of Chemistry, G.R.D.-IMT College, Dehradun-248001, India
[3]Department of Chemistry, Dr. S.N.N. Government Degree College, Vedikhal Pauri Garhwal-246177, India

*Corresponding author: E-mail: dpasaini91@gmail.com

Received: 13 November 2025 *Accepted*: 15 January 2026 *Published online*: 6 March 2026 AJC-22287

In this work, palladium and iridium monometallic nanoparticles (MMNPs), along with their bimetallic counterparts (BMNPs) in different ratios 1:1, 2:1 and 1:2, were synthesised using the green-mediated scheme by employing *Murraya koenigii* leaf extract, a medicinal plant rich in bioactive compounds such as flavonoids with known antibacterial and anticancer properties. The consequent nanoparticles were characterised by several techniques including UV-visible absorption (UV-Vis), X-ray diffraction (XRD), field-emission scanning electron microscopy (FE-SEM), high-resolution transmission electron microscopy (HR-TEM), Fourier transform infrared spectroscopy (FTIR), thermal analysis (TGA, DTA and DTG) and X-ray photoelectron spectroscopy (XPS). The XRD analysis confirmed the formation of PdO, IrO_2, along with Pd-Ir BMNPs. Further, the antibacterial efficacy of PdO, IrO_2 and Pd-Ir nanoparticles was evaluated along with Gram-positive (*Staphylococcus aureus*) and Gram-negative (*Pseudomonas aeruginosa*) bacteria. Notably, PdO MMNPs exhibited superior antibacterial activity against *Pseudomonas* with an inhibition zone of ± 9.33 mm at a 50 μg/mL concentration. Moreover, both mono- and bimetallic nanoparticles were assessed for their cytotoxic effects on the MCF-7 breast cancer cell line, where IrO_2 MMNPs demonstrated the most potent anticancer properties, yielding an IC_{50} value of 236.8 ± 0.12 μg/mL.

Keywords: Antibacterial activity, Anticancer activity, *Murraya koenigii*, Monometallic nanoparticles, Bimetallic nanoparticles.

INTRODUCTION

Nanotechnology is a rapidly growing research area valued for its unique properties and applications in agriculture, food and healthcare [1,2]. Metal nanoparticles such as magnesium, zinc, copper, platinum and silver are especially studied for their diverse therapeutic potential in biomedicine [3,4]. Modifying nanoparticles into bimetallic structures markedly improves their optical, catalytic and structural performance, often generating novel or enhanced functionalities across multiple applications [5]. To meet growing interest in these materials, researchers increasingly employ plant-based green synthesis methods as sustainable alternatives to conventional chemical or hydrothermal approaches [6,7]. These eco-friendly strategies minimize toxic reagents, reduce harmful waste, simplify processing and use natural biomolecules as stabilizing and reducing agents. Plant constituents such as flavonoids, terpenoids and polyphenols play a central role by facilitating nanoparticle formation through their strong reducing capacity [8,9]. These compounds act as capping agents that stabilize nanoparticles and as reducing agents that provide electrons to metal ions, forming metal atoms at the nanoscale [10]. Furthermore, these phytochemicals stabilize various bimetallic nanoparticles (BMNPs) through electrostatic repulsion and spatial resistance [11].

Among various plant-based approaches, *Murraya koenigii* leaf is classified in the Rutaceae family, also known as Karipatta, curry leaves, Tulu Bevusoppu, Meethi neem, Mitho limado, Kariveppilai, Kariveppu, Girinimba, Karibevu, Karepeku (India), Folhas de caril (Portugal), Listya karri (Russia), Fogli di Cari (Spain), Hojas de curry (Spanish) and several others [12]. *M. koenigii* leaf extract possesses a wide range of pharmacological properties, such as antidiabetic [13], anticancer [14-16], antimicrobial [17], antidermatophyte, antioxidant [18,19], antihypertensive, mosquitocidal, antifungal, larvicidal, anti-allergic, hepatoprotective [12], anti-mutagenic [20], anti-inflammatory [21] and antibacterial [22] activities.

BMNPs are a classification of materials that exhibit a combination of traits related to the two constituent metals. Due to synergistic effects, there is often a significant enhancement in their unique physical and chemical characteristics [23]. Through electrical, geometrical and mixed sites, bimetallicity can increase the activity, selectivity and stability of monometals [24]. Thus, in this study, a green synthesis approach was used to synthesize PdO, IrO_2 MMNPs and Pd-Ir (1:1, 2:1 and 1:2) BMNPs. All the synthesized nanoparticles were characterized using various analytical techniques, including UV-visible spectroscopy, XRD, FE-SEM, TEM, XPS, TGA, DTA and DSC. Their antibacterial efficacy was evaluated against both Gram-positive and Gram-negative bacteria, focusing on PdO, IrO_2 and Pd-Ir nanoparticles. Additionally, their anticancer potential was assessed against the MCF-7 breast cancer cell line.

EXPERIMENTAL

All the chemicals and reagents for the synthesis were of analytical (AR) grade and used without any additional purification steps. Palladium chloride ($PdCl_2$), iridium trichloride ($IrCl_3$) and precursor salts were procured from Sisco Research Laboratory, India. Sodium hydroxide (NaOH) pellets were obtained from Merck Ltd., India.

Preparation of leaf extract: *Murraya koenigii* leaves were collected from the garden field of Gurukul Kangri (Deemed to be University), Haridwar, India and verified by the Patanjali Research Institute, Haridwar, India. To prepare the extract, fresh *M. koenigii* leaves were adequately washed in double-distilled water and left to dry for a week. About 5 g of dried leaves were boiled in 100 mL of double-distilled water for 30 min, then filtered and cooled to obtain the plant leaf extract. This extract served as a reducing agent during the synthesis of the NPs. This extract contains various types of secondary metabolites that act as reducing agents during the synthesis reaction of NPs. After that the PdO, IrO_2 MMNPs and Pd-Ir BMNPs are synthesised using the filtered extract.

Synthesis of monometallic (PdO, IrO_2) and bimetallic Pd-Ir NPs: PdO and IrO_2 MMNPs and Pd-Ir BMNPs were synthesised using the standard method *i.e.* 50 mL of *M. koenigii* leaf aqueous extract was added dropwise into precursor salts solution, 200 mL of 2.77×10^{-3} M $PdCl_2$ and 1.53×10^{-3} M $IrCl_3$ into two separate beakers. For case of Pd-Ir BMNPs, 50 mL of *M. koenigii* leaf aqueous extract was added dropwise into an equimolar 200 mL mixture of $IrCl_3$ and $PdCl_2$ precursor salts. This mixture was afterward kept on a hot plate with magnetic stirring for 1 h at 80 ºC. Consequently, the visible colour transform of the solution from light green to brown, revealing the formation of nanoparticles. To the proven, the UV-Vis absorption spectra were monitored, showing the formation of nanoparticles. Further, the colloidal solution was centrifuged at 15000 rpm for 15 min. This colloidal solution was washed with distilled water and dried in an electric oven at 90-100 ºC to collect the powdered form of nanoparticles. Thus, black powder undergoes further characterisation using different techniques for the confirmation of the synthesised nanoparticles.

Characterisation: X-ray diffraction spectroscopy (Panalytical's X'pert Pro) technique was adopted to investigate the morphological and structural analysis of nanoparticles. FT-IR spectra were recorded (Tensor 27, BRUKER) using the KBr pellets in the range of 4000-400 cm^{-1}. As well as the FE-SEM (Hitachi H-7500) technique was employed to examine the morphological characteristics of the synthesised nanoparticles. The HR-TEM (Hitachi H-7500) technique was used to calculate crystallite size. The double-beam (Systronics-2203) spectrophotometer was used to investigate the progress of nanoparticles formation. XPS (PHI 5000 Versa Probe III) spectra were measured to determine the chemical composition as well oxidation state of the Pd-Ir BMNPs sample. TGA, DTA and DTG (SII 6300 EXSTAR) techniques were applied at a constant heating rate of 10 ºC/min over a temperature range of 10-1000 ºC to cover the reference material alumina powder.

RESULTS AND DISCUSSION

UV-Vis spectroscopy: To monitor the progress of reactions and authenticate the successful reduction of metal ions, leading to the synthesis of *M. koenigii* leaf-assisted nanocrystals, spectroscopy was used. The recorded absorption spectra of PdO, IrO_2 MMNPs and Pd-Ir BMNPs (1:1, 2:1 and 1:2) are shown in Fig. 1, respectively, while the absorption band of *M. koenigii* leaf extract is depicted in Fig. 1f [25]. In case of MMNPs, Fig. 1a-b illustrate the absorption bands of precursor salts ($PdCl_2$ or $IrCl_3$) reaction mixture, which initially exhibit stable peaks at 372 nm and 329 nm, respectively. Following the reduction reaction taking place by *M. koenigii* leaf extract, these peaks shift to 377 nm and 387 nm, indicating flourishing nanoparticle formation. Similarly, in BMNPs, Fig. 1c represents Pd-Ir (1:1), Fig. 1d Pd-Ir (2:1) and Fig. 1e Pd-Ir (1:2), with original peaks at 274 nm, 375 nm and 329 nm. After reduction with *M. koenigii* leaf extract, these peaks shift to 372 nm, 380 nm and 368 nm, respectively, confirming structural modifications induced by the plant extract. In Fig. 1f, the *M. koenigii* leaf extract exhibits an absorption band near 312 nm. Initial peaks disappear and gradually shift to nanoparticles, indicating that the *M. koenigii* leaf extract forms metal nanoparticles. This reaction is further evidenced by a significant colour change in the solution from greenish to pale brown [23], signifying the reduction of metal ions and the formation of newly formed nanostructures.

XRD studies: The XRD spectra of PdO, IrO_2 MMNPs and Pd-Ir BMNPs are shown in Fig. 2. The stabilised nano PdO shows four peaks at 2θ, close to 34º, 40º, 46º and 68º, with the reflection planes (002), (111), (200) and (220), respectively. The stabilised nano IrO_2 shows six peaks at 2θ, close to 35º, 40º, 56º, 58º, 68º and 74º in Fig. 2a. The broad peaks around 35º, 40º, 56º, 58º, 68º and 74º show the reflection planes (101), (111), (210), (211), (220) and (202), respectively, which are characteristics of isolated IrO_2 nanoparticles. The broad diffraction peaks indicate the amorphous character of the samples [26]. The XRD spectra of Pd-Ir BMNPs (1:1) showed four peaks at 2θ around 34º, 39º, 46º and 67º. The peaks at 35º, 40º and 68º, showing in the reflection (Fig. 2c), are shifted to 34º, 39º and 67º, respectively. The diffraction peaks of oxides Pd-Ir BMNPs shift slightly to higher 2θ values when compared to the peaks of IrO_2 MMNPs, indicating that PdO has penetrated the IrO_2 lattice to create the Pd-Ir alloy

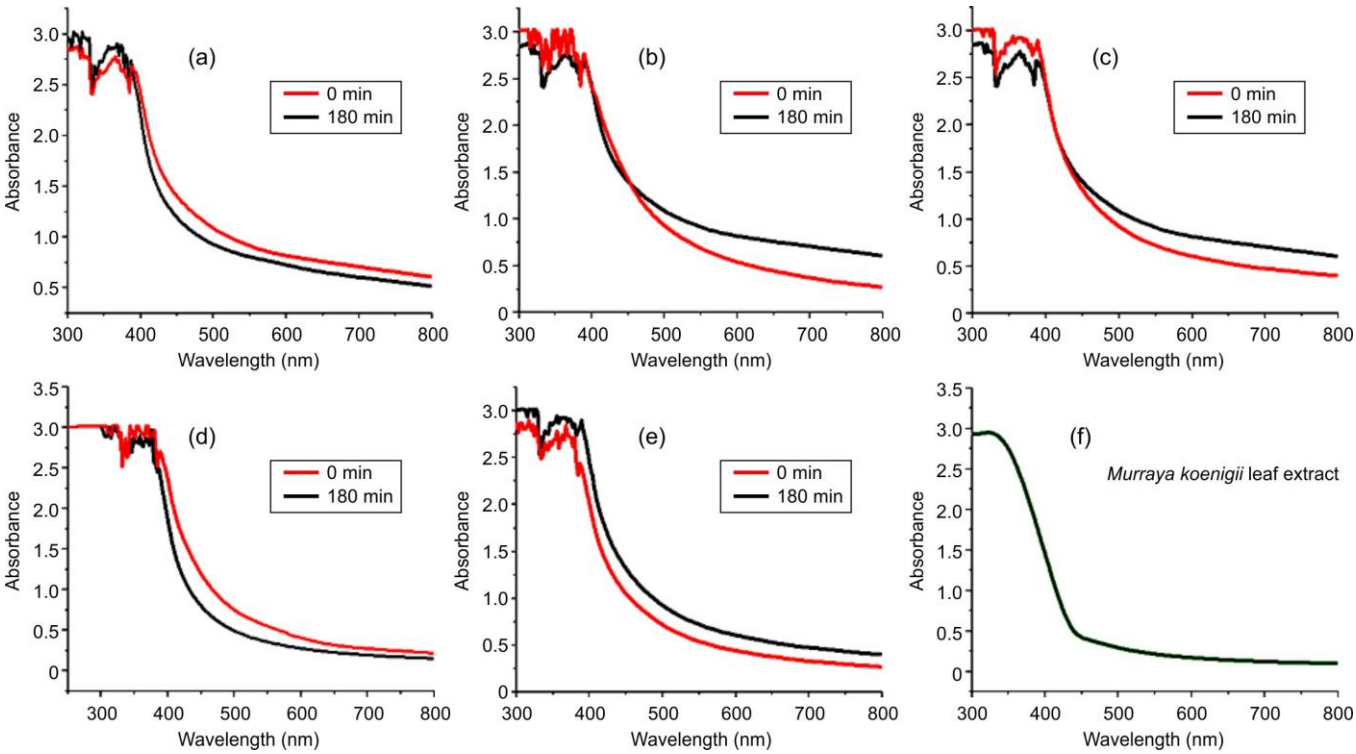

Fig. 1. UV-Vis spectra of (a) PdO, (b) IrO_2 MMNPs, (c) Pd-Ir (1:1), (d) Pd-Ir (2:1), (e) Pd-Ir (1:2) BMNPs, (f) *M. koenigii* leaf extract

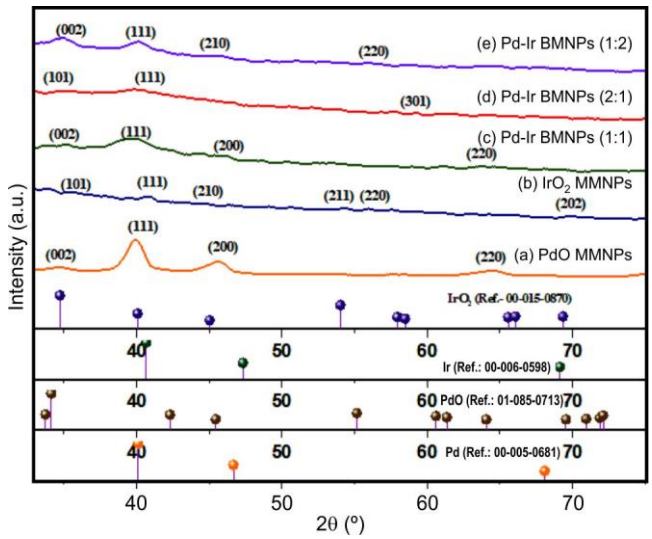

Fig. 2. XRD spectra of (a) PdO MMNPs, (b) IrO_2 MMNPs, (c) Pd-Ir (1:1), (d) Pd-Ir (2:1), and (e) Pd-Ir (1:2) BMNPs

form. XRD spectra of Pd-Ir (2:1) BMNPs demonstrate three peaks at 2θ close to 34º, 39º and 60º. The peaks at 35º and 58º in image (Fig. 2d) are shifted to 34º and 60º due to the high concentration of IrO_2, which moves towards IrO_2 MMNPs. XRD spectra of Pd-Ir (1:2) BMNPs illustrate four peaks at 2θ close to 34º, 39º, 46º and 58º, whereas the peaks at 34º and 39º in the image (Fig. 2e) are shifted to 35º and 40º. This is due to the high concentration of IrO_2 [27], which reallocates towards PdO MMNPs. The XRD spectra of the IrO_2 MMNPs, displayed with their JCPDS card no. 00-015-0870, confirm the tetragonal structure and phase of the sample [23]. The PdO MMNPs X-ray pattern, displayed with its JCPDS card no. 01-085-0713, confirms the tetragonal structure and phase of the sample. The peak of BMNPs (Pd-Ir) precisely corresponds to the PdO and IrO_2 MMNPs (with the JCPDS card nos. 00-006-0598 and 00-005-0681, respectively [28,29]. The approximate crystalline size was calculated using the Debye-Scherrer eqn:

$$Dc = \frac{K\lambda}{\beta \cos\theta}$$

where D is the average crystallite size; K is the shape factor; λ is the X-ray wavelength; β is the FWHM (full width of the diffraction peak at half maximum intensity) and θ is the Bragg angle [30]. For the PdO, IrO_2 and Pd-Ir (1:1), (2:1) and (1:2) samples, the estimated crystallite sizes are 5.9, 9.8, 3.3, 5.0 and 4.8 nm, respectively. The crystallite size results show that the Pd-Ir (1:1) sample has smaller crystallite sizes than the (2:1) and (1:2) samples, which is due to the interaction between iridium and palladium bimetallic nanoparticles.

FTIR studies: The FTIR spectra of Pd-Ir (1:1), Pd-Ir (2:1) and Pd-Ir (1:2) BMNPs are shown as Fig. 3. The bands at 3614 cm^{-1} in the Pd-Ir (1:1), 3681 cm^{-1} in the Pd-Ir (2:1) and 3675 cm^{-1} in the Pd-Ir (1:2) spectra are due to the –OH stretching, which are shifted from 3225 cm^{-1} in the *M. koenigii* leaf extract spectra. The literature reveals that the FTIR spectra of *M. koenigii* leaf extract show bands at 3225 cm^{-1}, which indicates that the extract contains moisture and polyphenols that confirm the presence of O–H stretching [31]. Another band, correlated to the amine group in the carbazole alkaloids that acts as a reducing agent during the formation of nanoparticles. Additional peaks have also been observed at 1645 cm^{-1}, which indicates the presence of cinnamaldehyde and the stretching modes –C=O, which are shifted to (a) 1545 cm^{-1}, (b) 1594 cm^{-1} and (c) 1592 cm^{-1} [16]. The presence of cinna-

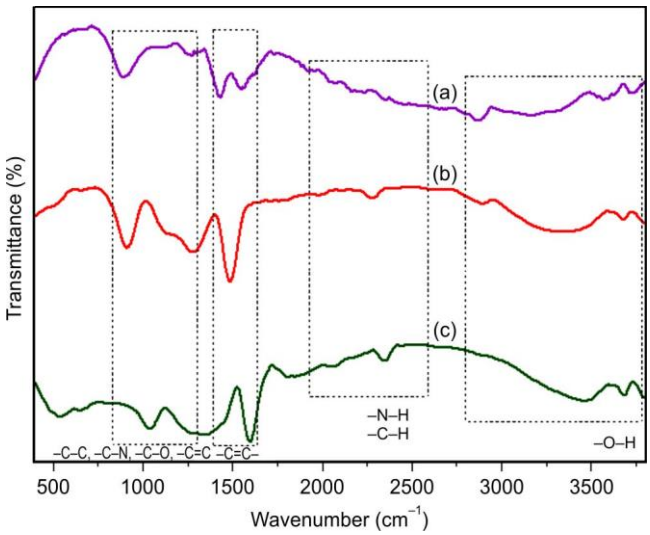

Fig. 3. FTIR spectra of (a) Pd-Ir (1:1), (b) Pd-Ir (2:1), (c) Pd-Ir (1:2) BMNPs

maldehyde acts as a capping agent, providing stability to the synthesised nanoparticles.

The presence of cinnamaldehyde works as a capping agent and provides stability to the synthesised nanoparticles. The bands at (a) 2412 cm^{-1}, (b) 2350 cm^{-1} and (c) 2346 cm^{-1} correspond to IrO_2, which is reported at 2378 cm^{-1} by Goel & Tomar [23]. The other bands at 3381 cm^{-1}, 3681 cm^{-1} and 3671 cm^{-1} show the presence of PdO [32,33]. The shifting of bands reveals some interaction between the extract and the oxides of Pd-Ir BMNPs.

FE-SEM studies: It has been observed from the FE-SEM images that the morphology of the Pd-Ir BMNPs samples changes when their elemental composition changes, as in case of the Pd-Ir BMNPs (1:1) sample, particles are irregular with some agglomeration in shape, while the Pd-Ir (2:1) and (1:2) are also irregular in shape. Bimetallic nanoparticles are aggregated with smooth surfaces. The elemental mapping and chemical composition of all samples were analysed using

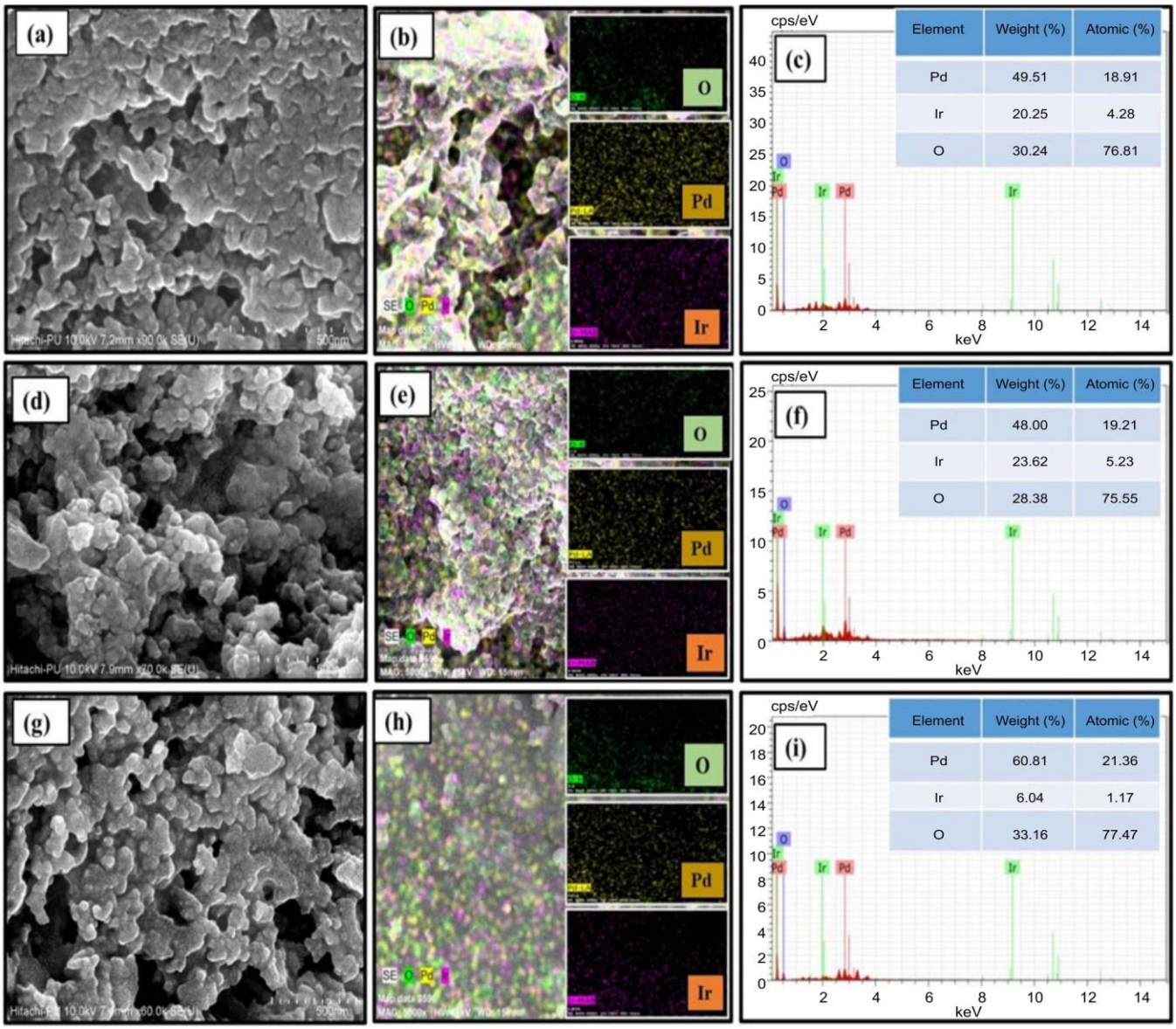

Fig. 4. FE-SEM, elemental mapping and EDAX of (a, b, c) Pd-Ir (1:1), (b, e, f) Pd-Ir (2:1), (g, h, i) Pd-Ir (1:2) BMNPs

EDAX, as shown in Fig. 4(b,c,e,f,h,i). The elemental mapping of all samples confirms equal distribution of elements throughout them. The Pd-Ir sample image is displayed in Fig. 4h confirmed the alloy form and provide evidence for the successful formation of bimetallic nanoparticles, as well as the excellent physical contact between the irregular-shaped PdO and IrO_2. The EDAX spectrum confirms the elements PdO, IrO_2 and O. In Fig. 4(c,f,i), the elemental composition percentage ratios for Pd-Ir (1:1), Pd-Ir (2:1) and Pd-Ir (1:2) were 71:29, 67:33 and 74:26, respectively [23].

HR-TEM analysis: For this perspective morphology and size of Pd-Ir BMNPs have been confirmed by the high-resolution study of the nanoparticles, conducted using HR-TEM. The nanoparticles micrograph and histograms are shown in Fig. 5. The HR-TEM images verified that the Pd-Ir BMNPs (1:1) are small in size and less distributed as compared to other (b) and (c) BMNPs (2:1 and 1:2 ratio) samples. From the HR-TEM images, the average crystallite size of the samples was determined to be less than 10 nm, *i.e.*, for Pd-Ir (1:1) - 2.91 nm, for Pd-Ir (2:1) - 6.60 nm and 5.08 nm for Pd-Ir (1:2) ratio of the samples based on the histogram graphs.

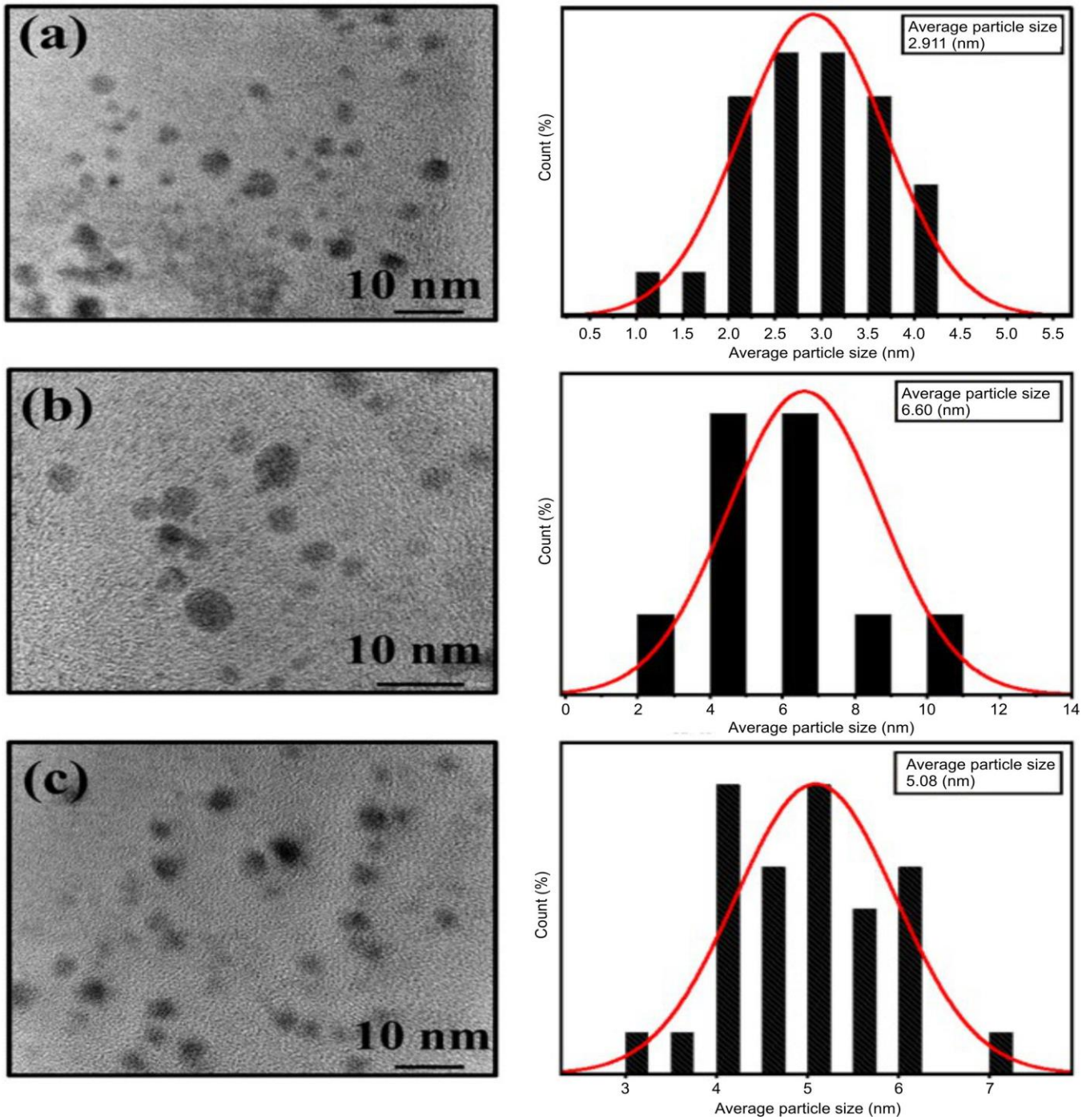

Fig. 5. HR-TEM images of (a) Pd-Ir (1:1), (b) Pd-Ir (2:1) and (c) Pd-Ir (1:2) BMNPs

XPS analysis: *M. koenigii* leaf extract mediated nanoparticles data are presented in the form of XPS spectrum for the Pd-Ir BMNPs, as shown in Fig. 6a-e. The XPS spectra of the Pd-Ir BMNPs sample confirm the presence of Pd, Ir, C and O, which are exposed during the survey scan. Besides this, the fitting of the PdO (3*d*) and IrO_2 (4*f*) spectra using XPS data is shown in Fig. 6b-c. The graph of the PdO (3d) spectra consists of two major peaks at binding energies of 337.5 eV and 342.9 eV [24]. The graph of the IrO_2 (4*f*) spectra shows the major peaks located at 62.2 eV and 65.09 eV, respectively. These values correspond to the (+4) oxidation state of Ir in IrO_2 and the (+2) oxidation state of Pd in the PdO sample. The C 1s and O1s element spectra in the Pd-Ir bimetallic sample are shown in Fig. 6d-e. The peaks of the C 1s and O1s elements are represented at 284.8 eV and 536.9 eV [34].

Thermal studies: TGA, DTA and DTG techniques were used to analyze the thermal behaviour of *M. koenigii* leaf extract-assisted Pd-Ir BMNPs. The results for all samples are shown in Fig. 7. The TGA of Pd-Ir BMNPs indicates that the samples undergo various stages of weight loss and degradation. The samples undergo an initial weight loss in the temperature range of 24-177 ºC for Pd-Ir (1:1), 32-150 ºC for Pd-Ir (2:1) and 32-154 ºC for Pd-Ir (1:2). The weight loss observed was 14.7% for Pd-Ir (1:1), 9.9% for Pd-Ir (2:1) and 6.8% for Pd-Ir (1:2) samples of their initial quantities, respectively. This weight loss is attributed to the evaporation of light volatiles and moisture. In DTG analysis, the Pd-Ir (1:1) sample exhibited initial weight loss between 24-289 ºC, with maximum loss at 289-668 ºC at rates of 0.136 and 0.073 mg/min. For Pd-Ir (2:1) and Pd-Ir (1:2), maximum weight losses occurred at 32-295 ºC (0.108 mg/min) and 32-207 ºC (62.6 mg/min), respectively. The second degradation stage occurred at 177-344 ºC for Pd-Ir (1:1), 150-343 ºC for Pd-Ir (2:1) and 154-341 ºC for Pd-Ir (1:2), with ~33-34% mass loss, attributed to the release of crystalline water and oxygen containing surface groups. The third stage, spanning 344-678 ºC (1:1), 343-515 ºC (2:1) and 341-995 ºC (1:2), caused 11-32% loss due to pyrolysis of aromatic compounds, oxidation and phytomolecules breakdown. The fourth stage occurred at 678-993 ºC (1:1) and 515-993 ºC (2:1) with ~11-13% degradation. DTA curves showed exothermic peaks at 352, 488, and 688 ºC (1:1); 422 and 504 ºC (2:1) and 419 and 469 ºC (1:2), respectively to combustion of residual organic matter, confirming exothermic decomposition [23].

Antibacterial activity: Using the agar-well diffusion technique, the antibacterial activity of PdO, IrO_2 MMNPs and Pd-Ir BMNPs has been investigated against Gram-positive (*S. aureus*) and Gram-negative (*P. aeruginosa*) bacteria. The stock solutions (50 and 100 µg/mL) of PdO, IrO_2 MMNPs and Pd-Ir BMNPs at varying concentrations were used to evaluate the antimicrobial activity during a 24 h incubation period at 37 ºC. The growth of restricted inhibitory zones surrounding the disks showed the strong antibacterial activity of the produced nanoparticles against the studied Gram-positive and Gram-negative bacteria. Among the bulk bacterial strains, the lower concentration (50 µg/mL) has excellent antibacterial activity. The data for lower and higher concentrations is presented in Table-1, which shows that the zone of inhibition of PdO, IrO_2 MMNPs and Pd-Ir BMNPs (1:1) against *S. aureus* were ±

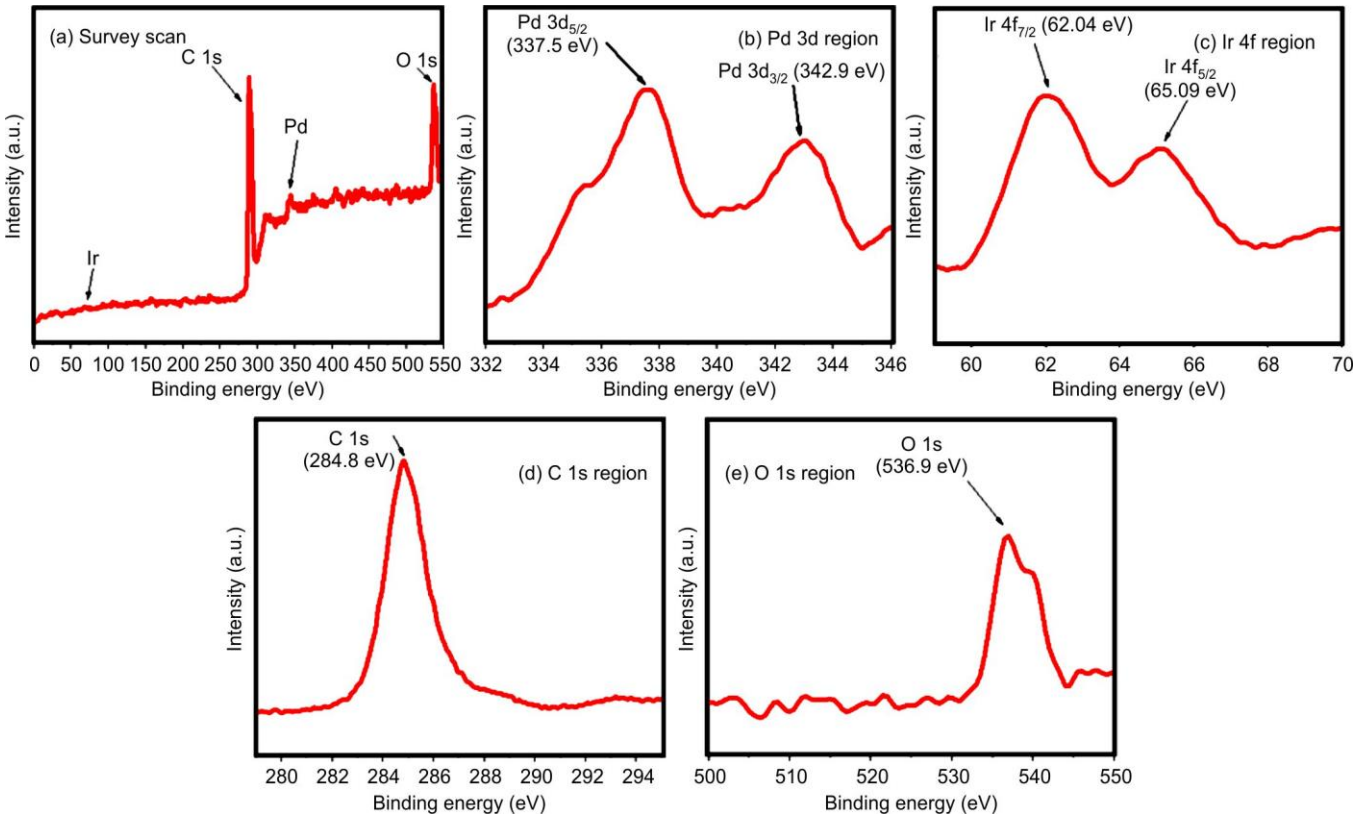

Fig. 6. XPS image of (a-d) Pd-Ir BMNPs (1:1), (2:1) and (1:2)

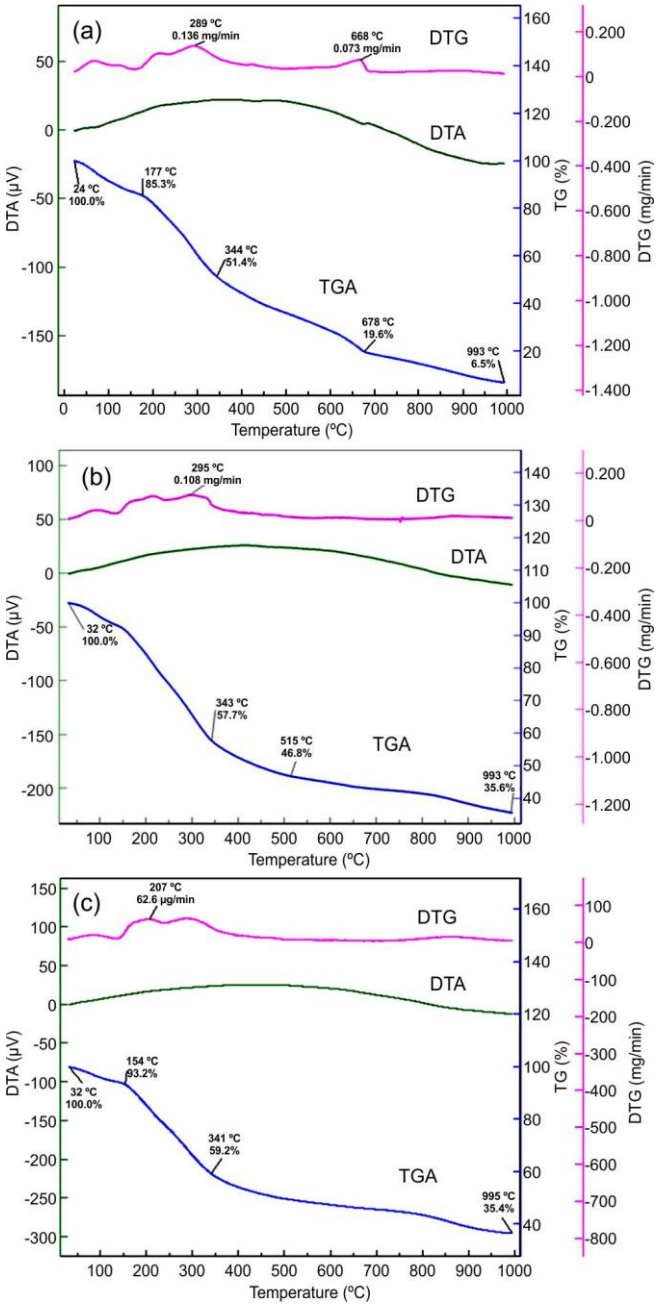

Fig. 7. TGA, DTA and DTG data of (a) Pd-Ir (1:1), (b) Pd-Ir (2:1), (c) Pd-Ir (1:2) BMNPs

TABLE-1
ANTIBACTERIAL ACTIVITY
DATA OF PdO, IrO_2 AND Pd-Ir (1:1)

Samples	Zone of inhibition (mm)			
	S. aureus		*P. aeruginosa*	
Conc. (μg/mL)	50	100	50	100
PdO MMNPs	± 5.56	± 5.0	± 9.33	± 8.8
IrO_2 MMNPs	± 4.26	± 2.4	± 6.16	± 6.0
Pd-Ir BMNPs (1:1)	± 2.73	± 2.6	± 4.43	± 3.9

5.56 mm, ± 9.33 mm and ± 4.26 mm, respectively and for *P. aeruginosa* were ± 6.16 mm and ± 2.73 mm and ± 4.43 mm, respectively. At the higher concentration (100 μg/mL), data in Table-1 show that the zone of inhibition of PdO, IrO_2 MMNPs and Pd-Ir (1:1) BMNPs against *S. aureus* ± 5 mm, ± 8.83 mm, ± 4.4 mm and for *P. aeruginosa* were ± 6.2 mm and ± 2.6 mm, ± 3.87 mm. Based on the results, PdO MMNPs show excellent antimicrobial activity against *P. aeruginosa* (± 9.33 mm at 50 μg/mL) [35].

Anticancer activity: The anticancer activity of the PdO, IrO_2 MMNPs and Pd-Ir (1:1) BMNPs on MCF-7 cell line was determined by MTT Assay. The cells (10000 cells/well) were incubated (Air-Jacketed CO_2 incubator, Heal Force-HF90) and 96-well plates for 24 h in DMEM medium (Dulbecco's modified eagle medium-AT149-1L, HIMEDIA) supplied with 10% FBS (fetal bovine serum, HIMEDIA-RM 10432) and 1% antibiotic solution (penicillin-streptomycin, Sigma-Aldrich P0781) with 5% CO_2 at 37ºC. The next day, cells were studied at various concentrations (10, 100, 500 and 1000 μg/mL) of the nanoparticle formulations. The sample stock solution was prepared in DMSO and subsequently diluted to form various concentrations in an incomplete cell culture medium (without FBS). Cells without sample MTT were considered blanks, whereas cells undergoing treatment were considered controls. The cell culture was grown for 24 h before adding MTT solution (5 mg/mL) and continued for 2 h. After the end of experiment, the cell layer substrate was dissolved in 100 μL of DMSO, the culture supernatant was collected and the plate reader ELISA (iMark, Biorad, USA) was used to measure the results at 540 nm. GraphPad Prism 6 software was used to calculate the IC_{50} [36]. The mean ± SD was used to present the results.

Based on the results obtained from the MTT assay, it was observed that when the MCF-7 cell line was defined to varied concentrations (10, 100, 500 and 1000 μg/mL) of the sample and standard, the cytotoxic activity was measured for sample PdO MMNPs (IC_{50} = 290.6 ± 0.18 μg/mL), IrO_2 MMNPs (IC_{50} = 236.8 ± 0.12 μg/mL), Pd-Ir BMNPs (1:1) (IC_{50} =524.5 ± 0.12 μg/mL) and standard capecitabine (IC_{50} = 339.2 ± 0.12 μM) given in Table-2. IrO_2 MMNPs were identified as the most cytotoxic among all these samples and standard capecitabine.

TABLE-2
ANTICANCER ACTIVITY DATA OF
PdO, IrO_2 AND Pd-Ir (1:1)

Sample	IC_{50} value (Mean ± SEM)
PdO MMNPs	290.6 ± 0.18 (μg/mL)
IrO_2 MMNPs	236.8 ± 0.12 (μg/mL)
Pd-Ir BMNPs (1:1)	524.5 ± 0.12 (μg/mL)
Capecitabine	339.2 ± 0.12 (μM)

To investigate the impact of anticancer therapy on breast cancer tumor cells, capecitabine medicine was chosen as the standard, along with the prepared nanoparticles (PdO, IrO_2 MMNPs and Pd-Ir BMNPs). The MCF-7 cells were grown in a single layer with different concentrations (10, 100, 500 and 1000 μg/mL) of NPs and standards to evaluate cell viability and the results are shown in Fig. 8. PdO MMNPs, cell viability was 71.08%, 58.13 %, 47.59% and 53.0%. IrO_2 MMNPs, cell viability was 81.85%, 58.69 %, 41.70% and 38.22%. The Pd-Ir BMNPs, cell viability was 85.60%, 70.04%, 60.70% and 41.63% and capecitabine (standard) cell viability was 75.84%, 61.07%, 47.99% and 47.65%. In Fig. 9, after the

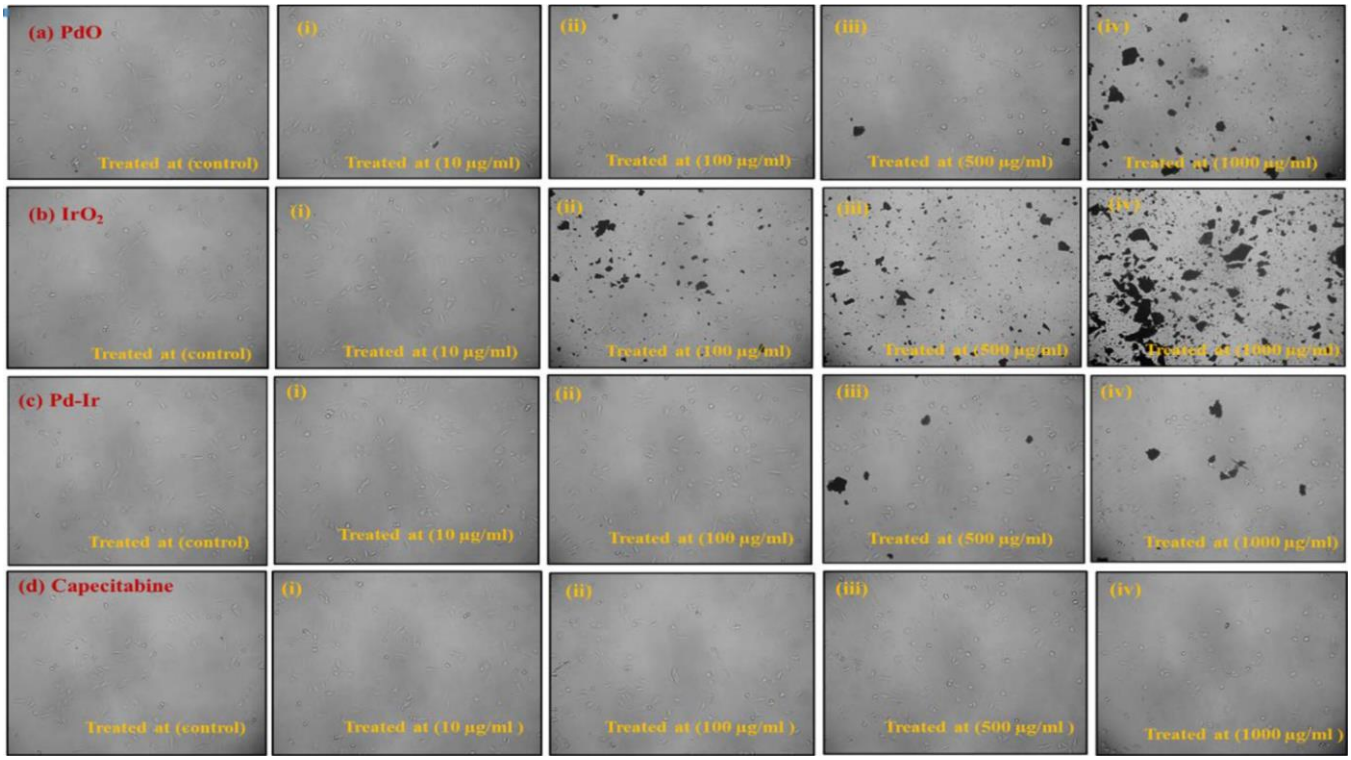

Fig. 8. Anticancer activity of (a) PdO, (b) IrO_2, MMNPs (c) Pd-Ir (1:1) BMNPs, and (d) Capecitabine (standard)

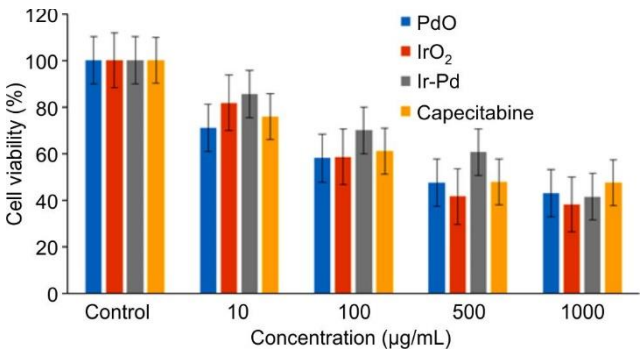

Fig. 9. Bar graph of MCF 7 cell lines anticancer drugs in PdO, IrO_2, Pd-Ir, and capecitabine (standard)

comparison between all PdO, IrO_2 MMNPs and Pd-Ir BMNPs, it was found that in the MCF7 cell lines at 10, 100, 500 and 1000 µg/mL, which was even better than standard capecitabine when compared to other PdO MMNPs and Pd-Ir BMNPs. IrO_2 MMNPs proved the most effective anticancer properties against breast cancer tumor cells (MCF-7) with an IC_{50} of 236.8 ± 0.12 (µg/mL).

Conclusion

This study successfully demonstrates the eco-friendly synthesis of Pd NPs, Ir NPs and Pd-Ir BMNPs using *Murraya koenigii* leaf extract and highlights its promising applications in pharmaceutical and biological aspects. The XRD analysis further verified their crystalline nature, reinforcing the structural integrity of the synthesised nanoparticles. To understand surface interactions, FTIR spectroscopy identified the presence of phytochemicals, which play a crucial role in nanoparticle stabilisation. Morphological analysis *via* FE-SEM revealed diverse particle structures, while elemental composition was authenticated through EDAX and elemental mapping, confirming the distribution of PdO and IrO_2. HR-TEM imaging provided precise crystallite size measurements of Pd-Ir BMNPs, with sizes determined as 2.91 nm, 6.60 nm and 5.08 nm for Pd-Ir BMNPs in the ratios 1:1, 2:1 and 1:2, respectively. Further analysis *via* XPS delineated the dual valence states of Pd-Ir NPs, where PdO exhibited $3d^0$ metallic and $3d^{2+}$ ionic states (5/2, 3/2) and IrO_2 showed $4f^0$ metallic and $4f^{4+}$ ionic states (7/2, 5/2). Stability assessments through thermal analysis indicated that Pd-Ir (1:1) displayed superior thermal stability compared to the (2:1) and (1:2) variants, with a recorded weight loss of 85.3% in TGA data. The biomedical potential of these nanoparticles was further evaluated through antibacterial and cytotoxicity studies. PdO MMNPs exhibited stronger antibacterial activity against both Gram-positive and Gram-negative bacteria compared to IrO_2 MMNPs and Pd-Ir BMNPs (1:1). Moreover, the cytotoxicity assessments revealed that IrO_2 MMNPs had higher toxicity levels than PdO MMNPs, Pd-Ir BMNPs (1:1) and the standard drug capecitabine, with a cell viability of 38.22% at 1000 µg/mL. Given these findings, future research could focus on surface modifications to enhance nanoparticle targeting capabilities for bacterial infections and cancer treatments. Thus, this study underscores an environmentally sustainable approach to nanoparticle synthesis, offering a viable pathway for biomedical applications.

ACKNOWLEDGEMENTS

The authors thank Gurukul Kangri (Deemed to be University), Haridwar, for providing the necessary facilities for this research work. The authors also acknowledge Panjab Uni-

versity, Chandigarh, for XRD, FESEM, EDAX, and HRTEM analyses; IIT Roorkee for XPS analysis; and IIT Indore for FTIR as well as TGA/DTA analyses.

CONFLICT OF INTEREST

The authors declare that there is no conflict of interests regarding the publication of this article.

DECLARATION OF AI-ASSISTED TECHNOLOGIES

During the preparation of this manuscript, the authors used an AI-assisted tool(s) to improve the language. The authors reviewed and edited the content and take full responsibility for the published work.

REFERENCES

1. S. Malik, K. Muhammad and Y. Waheed, *Molecules*, **28**, 661 (2023); https://doi.org/10.3390/molecules28020661
2. X. Ma, Y. Tian, R. Yang, H. Wang, L.W. Allahou, G. Williams, J. Chang, J.C. Knowles and A. Poma, *J. Nanobiotechnol.*, **22**, 715 (2024); https://doi.org/10.1186/s12951-024-02901-x
3. M. Rai, A.P. Ingle, S. Birla, A. Yadav and C.A. Dos Santos, *Crit. Rev. Microbiol.*, **42**, 696 (2016); https://doi.org/10.3109/1040841X.2015.1018131
4. N. Mahendran, B. Anand, M. Rajarajan, A. Muthuvel and V. Mohana, *Mater. Today Proc.*, **49**, 2620 (2022); https://doi.org/10.1016/j.matpr.2021.08.043
5. D.S. Idris and A. Roy, *Crystals*, **13**, 637 (2023); https://doi.org/10.3390/cryst13040637
6. R. Saxena, S. Kotnala, S.C. Bhatt, M. Uniyal, B.S. Rawat, P. Negi and M.K. Riyal, *Sustain. Chem. Climate Action*, **6**, 100071 (2025); https://doi.org/10.1016/j.scca.2025.100071
7. C. Hano and B.H. Abbasi, *Biomolecules*, **12**, 31 (2021); https://doi.org/10.3390/biom12010031
8. P.V. Kumar, K.S. Pushpavalli, B.G. Kumar, S.M. Jelastin Kala and K.S. Prakash, *Results Chem.*, **13**, 101945 (2025); https://doi.org/10.1016/j.rechem.2024.101945
9. L. Liu, C. Yu, S. Ahmad, C. Ri and J. Tang, *J. Environ. Manage.*, **344**, 118546 (2023); https://doi.org/10.1016/j.jenvman.2023.118546
10. A. Bhardwaj, Ritika and A.K. Singh, *Plant Nano Biol.*, **8**, 100076 (2024); https://doi.org/10.1016/j.plana.2024.100076
11. A.S. Aliero, S.H. Hasmoni, A. Haruna, M. Isah, N.A.N.N. Malek and N.A. Zawawi, *Emerg. Contam.*, **11**, 100411 (2025); https://doi.org/10.1016/j.emcon.2024.100411
12. P. Suthar, S. Kumar, V. Kumar, D. Vaidya, A. Sharma and A. Sharma, *S. Afr. J. Bot.*, **145**, 111 (2022); https://doi.org/10.1016/j.sajb.2021.11.025
13. D.S. Arumai Selvan, R.S. Kumar, S. Murugesan, S. Shobana and A.K. Rahiman, *J. Drug Deliv. Sci. Technol.*, **67**, 102838 (2022); https://doi.org/10.1016/j.jddst.2021.102838
14. S.K. Samanta, R. Kandimalla, B. Gogoi, K.N. Dutta, P. Choudhury, P.K. Deb, R. Devi, B.C. Pal and N.C. Talukdar, *Pharmacol. Res.*, **129**, 227 (2018); https://doi.org/10.1016/j.phrs.2017.11.024
15. A. Arun, O.P. Patel, D. Saini, P.P. Yadav and R. Konwar, *Biomed. Pharmacother.*, **93**, 510 (2017); https://doi.org/10.1016/j.biopha.2017.06.065
16. C. Kamaraj, G. Balasubramani, C. Siva, M. Raja, V. Balasubramanian, R.K. Raja, S. Tamilselvan, G. Benelli and P. Perumal, *J. Cluster Sci.*, **28**, 1667 (2017); https://doi.org/10.1007/s10876-017-1180-6
17. M. Vats, H. Singh and S. Sardana, *Braz. J. Microbiol.*, **42**, 1569 (2011); https://doi.org/10.1590/S1517-83822011000400044
18. A.K. Biswas, M.K. Chatli and J. Sahoo, *Food Chem.*, **133**, 467 (2012); https://doi.org/10.1016/j.foodchem.2012.01.073
19. B.Y. Aju, R. Rajalakshmi and S. Mini, *J. Pharmacogn. Phytochem.*, **6**, 939 (2017); https://doi.org/10.47413/vidya.v3i1.322
20. K. Ahmad, S.P. Tan, M.A. Sukari, A.M. Ali and M.A. Nafiah, *Am. J. Plant Sci.*, **5**, 2869 (2014); https://doi.org/10.4236/ajps.2014.519302
21. L.G. Prasad, V.K. Dua and A. Mathur, *Int. J. Pharm. Biol. Sci.*, **2**, 541 (2011).
22. I. Abuga, S.F. Sulaiman, R. Abdul Wahab, K.L. Ooi and M.S.B. Abdull Rasad, *Eur. J. Integr. Med.*, **33**, 101010 (2020); https://doi.org/10.1016/j.eujim.2019.101010
23. A. Goel and S. Tomar, *Inorg. Nano-Met. Chem.*, **54**, 342 (2024); https://doi.org/10.1080/24701556.2022.2034016
24. S. Ying, Z. Guan, P.C. Ofoegbu, P. Clubb, C. Rico, F. He and J. Hong, *Environ. Technol. Innov.*, **26**, 102336 (2022); https://doi.org/10.1016/j.eti.2022.102336
25. S. Kundu and H. Liang, *J. Colloid Interface Sci.*, **354**, 597 (2011); https://doi.org/10.1016/j.jcis.2010.11.032
26. B. Şen, A. Aygün, A. Şavk, S. Akocak and F. Şen, *Int. J. Hydrogen Energy*, **43**, 20183 (2018); https://doi.org/10.1016/j.ijhydene.2018.07.081
27. T.I. Asanova, I.P. Asanov, M.G. Kim, E.Y. Gerasimov, A.V. Zadesenets, P.E. Plyusnin and S.V. Korenev, *J. Nanopart. Res.*, **15**, 1994 (2013); https://doi.org/10.1007/s11051-013-1994-6
28. S. Saipanya, P. Waenkaew, S. Maturost, N. Pongpichayakul, O. Namsar, N. Promsawan, S. Kuimalee, K. Income, S. Themsirimongkon, B. Kuntalue, and J. Jakmunee, *ACS Omega*, **7**, 17741 (2022); https://doi.org/10.1021/acsomega.2c00906
29. J. Saffari, N. Mir, D. Ghanbari, K. Khandan-Barani, A. Hassanabadi and M.R. Hosseini-Tabatabaei, *J. Mater. Sci. Mater. Electron.*, **26**, 9591 (2015); https://doi.org/10.1007/s10854-015-3622-y
30. A. Goel, S. Shikha, S. Shivani and S. Tomar, *Curr. Chem. Lett.*, **10**, 209 (2021); https://doi.org/10.5267/j.ccl.2021.1.005
31. A. Aniqa and S. Kaur, *J. Drug Res. Ayurvedic Sci.*, **9**, 273 (2024); https://doi.org/10.4103/jdras.jdras_397_23
32. K. Elumalai, S. Velmurugan, V. Kathiravan, S. Ashokkumar and S. Ravi, *Mater. Sci. Semicond. Process.*, **34**, 365 (2015); https://doi.org/10.1016/j.mssp.2015.01.048
33. D. Philip, C. Unni, S.A. Aromal and V.K. Vidhu, *Spectrochim. Acta A Mol. Biomol. Spectrosc.*, **78**, 899 (2011); https://doi.org/10.1016/j.saa.2010.12.060
34. A. Goel, Abhilasha and Shivani, *Inorg. Nano-Met. Chem.*, **51**, 366 (2020); https://doi.org/10.1080/24701556.2020.1790001
35. G. Sharmila, M.F. Fathima, S. Haries, S. Geetha, N. Manoj Kumar and C. Muthukumaran, *J. Mol. Struct.*, **1138**, 35 (2017); https://doi.org/10.1016/j.molstruc.2017.02.097
36. G. Fotakis and J.A. Timbrell, *Toxicol. Lett.*, **160**, 171 (2006); https://doi.org/10.1016/j.toxlet.2005.07.001